

# We are IntechOpen, the world's leading publisher of Open Access books Built by scientists, for scientists

6,900

Open access books available

186,000

International authors and editors

200M

Downloads

Our authors are among the

154

Countries delivered to

TOP 1%

most cited scientists

12.2%

Contributors from top 500 universities



WEB OF SCIENCE™

Selection of our books indexed in the Book Citation Index  
in Web of Science™ Core Collection (BKCI)

Interested in publishing with us?  
Contact [book.department@intechopen.com](mailto:book.department@intechopen.com)

Numbers displayed above are based on latest data collected.  
For more information visit [www.intechopen.com](http://www.intechopen.com)



---

# Structure and Mechanical Behaviour of Cu-Zr-Ni-Al Amorphous Alloys Produced by Rapid Solidification

---

Celal Kursun and Musa Gogebakan

Additional information is available at the end of the chapter

<http://dx.doi.org/10.5772/63513>

---

## Abstract

The amorphous ribbons of  $\text{Cu}_{50}\text{Zr}_{40}\text{Ni}_5\text{Al}_5$  alloy were manufactured by rapid solidification. The ribbons were investigated by X-ray diffraction (XRD), scanning electron microscopy coupled with energy dispersive spectroscopy (SEM-EDX) and differential scanning calorimetry (DSC). The activation energy of the crystallisation in amorphous alloys was determined by Kissinger technique. The mechanical properties of the ribbons were characterized using Vickers microhardness (HV) tester. According to the XRD and SEM results, the  $\text{Cu}_{50}\text{Zr}_{40}\text{Ni}_5\text{Al}_5$  alloys have a fully amorphous structure. The EDX analysis of the ribbons showed that compositional homogeneity of the  $\text{Cu}_{50}\text{Zr}_{40}\text{Ni}_5\text{Al}_5$  alloy was fairly high. From the DSC curves of the amorphous ribbons, it was determined that glass transition temperature ( $T_g$ ) is around 440–442°C and super-cooled liquid region ( $\Delta T_x = T_x - T_s$ ) before crystallisation is around 61–64°C. The microhardness of the as-quenched ribbons was measured about 550 HV. However, this microhardness value decreased with increasing annealing temperature and it was calculated about 465 HV after annealing temperature of 800°C.

**Keywords:** rapid solidification, microhardness, copper-based alloy, crystallisation, Kissinger plot

---

## 1. Introduction

Amorphous alloys, with high corrosion resistant, ultrahigh strength and soft ferromagnetic and mechanical properties, have widely been the subject of intense investigation [1–4]. These excellent properties stem from their high chemical and structural homogeneous creation. Besides, it is possible to synthesise the amorphous alloys without restriction a wide chemical composition range. Amorphous alloys are used in many applications such as defence, electri-

cal, welding, automobile and aircrafts industries. Cu-based amorphous alloys are optimal materials because of their excellent mechanical properties and high electrical and thermal conductivities for these applications [5, 6]. In addition to these applications, copper alloys are also used as the rocket nozzles, high-performance switches, the heat exchangers, the condenser tubes of ships [7, 8].

Cu-based amorphous alloys can be produced by many different techniques such as rapid solidification, mechanical alloying, vapour depositions, plasma processing and solid state reactions. In the rapid solidification method, the amorphous alloys are manufactured on thin ribbons forms, which are usually ductile and bright surface. Many Cu-based binary, ternary, quaternary and quinary alloys have been manufactured by these methods [9–15]. In this work, Cu-Zr-Ni-Al quaternary amorphous alloys are produced by rapid solidification technique at wheel surface velocities of 35 and 41 ms<sup>-1</sup> as ribbons forms with very flexible. The effects of the wheel surface velocities and different annealing process on mechanical and microstructural properties of produced ribbons are systematically investigated. Therefore, it has been revealed the amorphous nature of Cu<sub>50</sub>Zr<sub>40</sub>Ni<sub>5</sub>Al<sub>5</sub> ribbon alloys in order to contribute the continuously improving Cu-based alloys in industry.

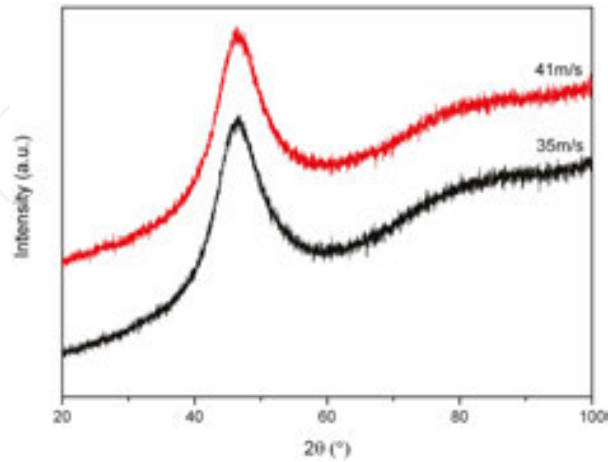
## 2. Methods and materials

An ingot of the Cu<sub>50</sub>Zr<sub>40</sub>Ni<sub>5</sub>Al<sub>5</sub> (at.%) alloy was prepared by arc melting the mixtures of the pure elements, Cu (99.7%), Zr (99.9%), Ni (99.5%) and Al (99.99%) in a titanium-gettered argon atmosphere. From this alloy, ribbon materials of approximately 75 μm thickness and 5 mm in width were manufactured by a single-roller Edmund Bühler melt spinner at wheel surface velocities of 35 and 41 ms<sup>-1</sup>. The structure of the ribbon samples was examined by XRD using a Philips X'Pert powder diffractometer with Cu-Kα radiation generated at 40 kV and 30 mA. The transformations temperatures and heat effects during transformations were examined by Perkin-Elmer Sapphire DSC unit under inert gas atmosphere using continuous heating mode with the heating rate of 40 K min<sup>-1</sup>. Moreover, the DSC analysis was carried out for the melt-spun ribbon at wheel speed of 35 ms<sup>-1</sup> using continuous heating mode with the heating rates of 5–40 K min<sup>-1</sup>. The cross section of the melt-spun ribbons was studied by Zeiss Evo LS10 SEM and SEM-EDX after conventional metallographic preparation. The ribbons were annealed for 30 min at different temperatures under vacuum/inert gas atmosphere. These temperature values are 300, 580, 680 and 800°C. The annealed ribbons were investigated by XRD from surface, SEM from cross-section with the same conditions used for as-quenched ribbons. The Vickers microhardness measurements of the as-quenched and subsequently annealed ribbons were performed using a Shimadzu HVM-2 by an applied load of 0.98 N with a dwell time of 10 s at ten different locations.

## 3. Results and Discussion

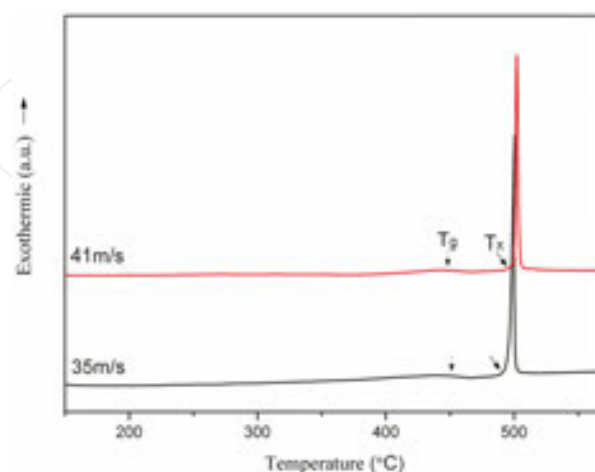
**Figure 1** shows the X-ray diffraction patterns of the rapidly solidified Cu<sub>50</sub>Zr<sub>40</sub>Ni<sub>5</sub>Al<sub>5</sub> ribbons produced at wheel surface velocities of 35 and 41 ms<sup>-1</sup>. As shown in **Figure 1**, the XRD patterns

exhibit the broad maxima characteristic which is feature of amorphous materials without the evidence of any crystalline peaks. This means that the surface velocities of 35 and 41  $\text{ms}^{-1}$  are optimal to synthesize  $\text{Cu}_{50}\text{Zr}_{40}\text{Ni}_5\text{Al}_5$  alloy as fully amorphous structure.



**Figure 1.** XRD pattern of the melt-spun  $\text{Cu}_{50}\text{Zr}_{40}\text{Ni}_5\text{Al}_5$  ribbons prepared at wheel speeds of 35 and 41  $\text{ms}^{-1}$  as-quenched.

DSC traces of amorphous  $\text{Cu}_{50}\text{Zr}_{40}\text{Ni}_5\text{Al}_5$  alloys at wheel speeds of 35 and 41  $\text{ms}^{-1}$  at a heating rate of 40  $\text{K min}^{-1}$  display distinct and an obvious glass transition temperature,  $T_g$ , before crystallisation, as shown in **Figure 2**. From the DSC curves, it is seen a wide super-cooled liquid temperature range followed by a pronounced exothermic reaction for both ribbon alloys. **Table 1** summarises the characteristic temperatures which are glass transition temperature ( $T_g$ ), crystallisation temperature ( $T_x$ ), super-cooled liquid region ( $\Delta T_x$  ( $\Delta T_x = T_x - T_g$ )), and peak temperature ( $T_p$ ) of the  $\text{Cu}_{50}\text{Zr}_{40}\text{Ni}_5\text{Al}_5$  alloy. According to the **Table 1**,  $T_x$ ,  $\Delta T_x$  and  $T_p$  increase while  $T_g$  decreases with increasing melt-spun wheel surface velocity.



**Figure 2.** The DSC curves of the  $\text{Cu}_{50}\text{Zr}_{40}\text{Ni}_5\text{Al}_5$  ribbon alloys at wheel speeds of 35 and 41  $\text{ms}^{-1}$  obtained during heating at a heating rate of 40  $\text{K min}^{-1}$ .

Wheel speed/ms <sup>-1</sup>	T <sub>g</sub> /°C	T <sub>x</sub> /°C	ΔT <sub>x</sub> /°C	T <sub>p</sub> /°C
35	442	503	61	507
41	440	504	64	509

**Table 1.** Thermal values obtained from DSC curves for melt-spun Cu<sub>50</sub>Zr<sub>40</sub>Ni<sub>5</sub>Al<sub>5</sub> ribbons at different wheel speed.

**Figure 3** exhibits the DSC curves at 5, 10, 20 and 40 K min<sup>-1</sup> of the ribbon alloy which are manufactured at wheel speeds of 35 ms<sup>-1</sup>. The obtained peak temperature values, T<sub>g</sub>, T<sub>x</sub>, T<sub>p</sub> and the super-cooled liquid region (ΔT<sub>x</sub>) from **Figure 3** are presented **Table 2**. As can be seen **Table 2**, T<sub>g</sub>, T<sub>x</sub>, T<sub>p</sub> and ΔT<sub>x</sub> values are moved to higher temperatures with increasing heating rate. It is attributed the heating rate which are depended on the parameters of crystallisation and glass transition during continuous heating [7, 16]. Therefore, this case reveals the significant of the kinetic aspects of the glass transition for glassy alloys [17].

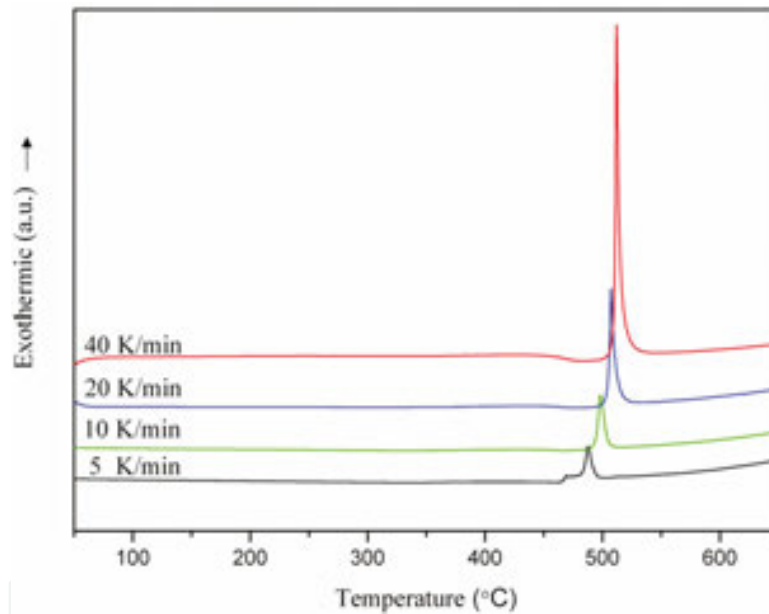


**Figure 3.** DSC analysis results for the melt-spun ribbon prepared at wheel speed of 35 ms<sup>-1</sup> using continuous heating mode with the heating rates of 5–40 K min<sup>-1</sup>.

φ (K/min)	T <sub>g</sub> /K	T <sub>x</sub> /K	ΔT <sub>x</sub> /K	T <sub>p</sub> /K
5	703	761	58	764
10	708	766	58	771
20	715	776	61	780
40	723	783	60	785

**Table 2.** Thermal values obtained from DSC curves for rapidly solidified Cu<sub>50</sub>Zr<sub>40</sub>Ni<sub>5</sub>Al<sub>5</sub> amorphous ribbons manufactured at wheel speed of 35 ms<sup>-1</sup> at different heating rates.

The activation energy ( $E$ ) for glass transition or crystallisation is commonly estimated by the Kissinger [18] equation. The Eq. (1) is given below. To calculate activation energy of the amorphous alloys with this equation, it is necessary to use data from different heating rates of the alloy

$$\ln\left(\frac{\phi}{T^2}\right) = -\frac{E}{RT} + A \quad (1)$$

where  $T$  is the specific temperature, glass transition temperature ( $T_g$ ), crystallisation temperature ( $T_x$ ), or peak temperature ( $T_p$ ), of crystallisation,  $\phi$  is the heating rate,  $R$  is the gas constant (8.314 J/mol K),  $E$  is the activation energy,  $A$  is a constant. By plotting  $\ln(\phi/T^2)$  versus  $1/(RT)$ , nearly a straight line is obtained. From the slope of this straight line, the activation energies  $E_g$ ,  $E_x$  or  $E_p$  are calculated using the certain peak temperatures ( $T_g$ ,  $T_x$ ,  $T_p$ ). **Figure 4** shows the Kissinger plots of  $\text{Cu}_{50}\text{Zr}_{40}\text{Ni}_5\text{Al}_5$  ribbon alloy produced at wheel speed of  $35 \text{ ms}^{-1}$ . From the Kissinger plots, the activation energies of  $E_g$ ,  $E_x$  and  $E_p$  are determined  $421.35 (\pm 12)$ ,  $432.26 (\pm 9)$  and  $403.05 (\pm 6)$  kJ/mol, respectively. These values are very high compared with previous studies whose activation energies are  $E_x = 393$ ,  $E_p = 381$  kJ/mol for  $\text{Cu}_{50}\text{Zr}_{40}\text{Ni}_5\text{Al}_5$  alloy [7],  $E_g = 357$ ,  $E_x = 297$ ,  $E_p = 289$  kJ/mol for  $\text{Cu}_{52.5}\text{Zr}_{11.5}\text{Ti}_{30}\text{Ni}_6$  [19] and  $E_g = 377$ ,  $E_x = 307$ ,  $E_p = 340$  kJ/mol for  $\text{Cu}_{45}\text{Zr}_{45}\text{Ag}_7\text{Al}_3$  alloy [20]. On the other hand, it is also possible to mention that the amorphous  $\text{Cu}_{50}\text{Zr}_{40}\text{Ni}_5\text{Al}_5$  alloy has very high thermodynamic stability with  $E_x = 432.26$  kJ/mol value compared with previous works.

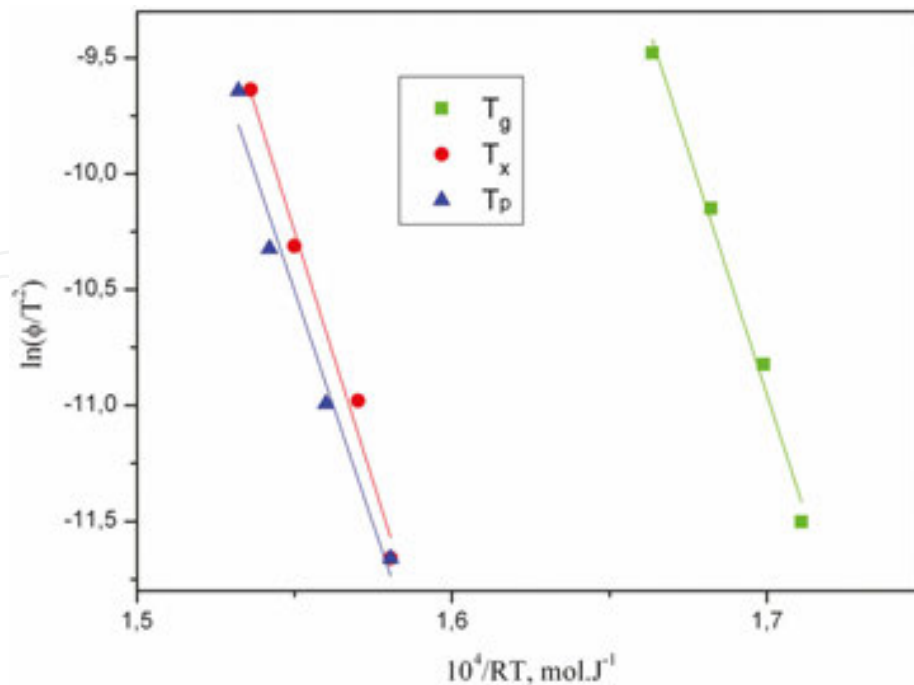


**Figure 4.** Kissinger plots of the amorphous  $\text{Cu}_{50}\text{Zr}_{40}\text{Ni}_5\text{Al}_5$  alloy produced at wheel speed of  $35 \text{ ms}^{-1}$ .

The annealing of the amorphous alloys is a significant process to characterise their crystallisation behaviour. Thus, it might be revealed that the amorphous structure transforms into what kind of crystalline phases with increasing annealing temperature. For this purpose, the melt-spun ribbon of  $\text{Cu}_{50}\text{Zr}_{40}\text{Ni}_5\text{Al}_5$  alloy synthesised at wheel speed of  $35 \text{ ms}^{-1}$  was annealed in the temperature range of  $300\text{--}800^\circ\text{C}$  for 30 min. **Figure 5** shows the XRD patterns of  $\text{Cu}_{50}\text{Zr}_{40}\text{Ni}_5\text{Al}_5$  alloy after annealing. According to **Figure 5**, before exothermic reaction, the XRD pattern of  $\text{Cu}_{50}\text{Zr}_{40}\text{Ni}_5\text{Al}_5$  alloy with annealed of  $300^\circ\text{C}$  exhibits fully an amorphous structure. After the annealing temperature of  $580^\circ\text{C}$ , intermetallic phases with sharp diffraction peaks have been obtained from the amorphous matrix and fully crystallisation of the amorphous phase. This result is in good agreement with crystallisation peak in DSC traces which is above  $503^\circ\text{C}$ . The obtained phases in the XRD spectrum were marked by symbols and indexed as cubic- $\text{AlCu}_2\text{Zr}$  with lattice parameters,  $a = b = c = 6215 \text{ \AA}$ , orthorhombic- $\text{Cu}_{10}\text{Zr}_7$  with lattice parameters,  $a = 9347$ ;  $b = 9322$ ;  $c = 12,976 \text{ \AA}$ , tetragonal- $\text{Zr}_2\text{Cu}$  with lattice parameters,  $a = 3220$ ;  $b = 3220$ ;  $c = 11,183 \text{ \AA}$  and f.c.c-Cu with lattice parameters,  $a = b = c = 3615 \text{ \AA}$ . These phases were also observed in previous works after a similar annealing process for Cu-based amorphous alloys [7, 20–22]. Number of the crystalline peaks which belongs to  $\text{AlCu}_2\text{Zr}$ ,  $\text{Cu}_{10}\text{Zr}_7$ ,  $\text{Zr}_2\text{Cu}$  and Cu phases was increased by increasing annealing temperature ( $800^\circ\text{C}$ ), as shown in **Figure 5**.

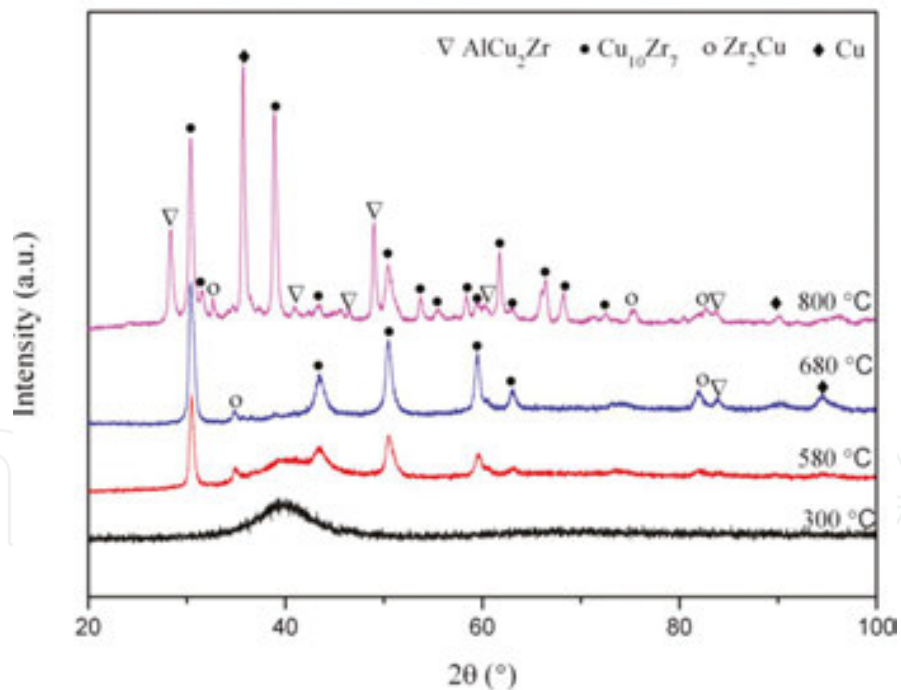


**Figure 5.** XRD pattern of the melt-spun ribbon of  $\text{Cu}_{50}\text{Zr}_{40}\text{Ni}_5\text{Al}_5$  alloy manufactured at a wheel speed of  $35 \text{ ms}^{-1}$  and annealed in the temperature range of  $200\text{--}800^\circ\text{C}$  for 30 min.

In addition to XRD patterns of annealed ribbons, typical SEM micrographs from cross section of the amorphous  $\text{Cu}_{50}\text{Zr}_{40}\text{Ni}_5\text{Al}_5$  alloy prepared at a wheel speed of  $35 \text{ ms}^{-1}$  as well as annealing ribbons at  $300$ ,  $580$ ,  $680$  and  $800^\circ\text{C}$  are shown in **Figure 6**. In **Figure 6a, b**, the microstructure

with featureless morphology of unannealed and annealed at 300°C ribbons are exhibited. This featureless morphology is a typical characteristic of the amorphous materials. In previous works, similar SEM images taken surface of amorphous structured materials were reported [7, 23, 24]. These micrographs are in accord with the XRD spectrums which exhibit fully amorphous features unannealed (**Figure 1**) and annealed at 300°C ribbons (**Figure 5**). As can be seen obviously in **Figure 6c–e**, with increasing annealing temperature (580, 680, 800°C), the microstructure of  $\text{Cu}_{50}\text{Zr}_{40}\text{Ni}_5\text{Al}_5$  ribbon alloys changes and transforms into irregularly shaped features which is a characteristic of crystalline structures. These crystalline structures belong to  $\text{AlCu}_2\text{Zr}$ ,  $\text{Cu}_{10}\text{Zr}_7$ ,  $\text{Zr}_2\text{Cu}$  or Cu phases obtained by XRD patterns (**Figure 5**)

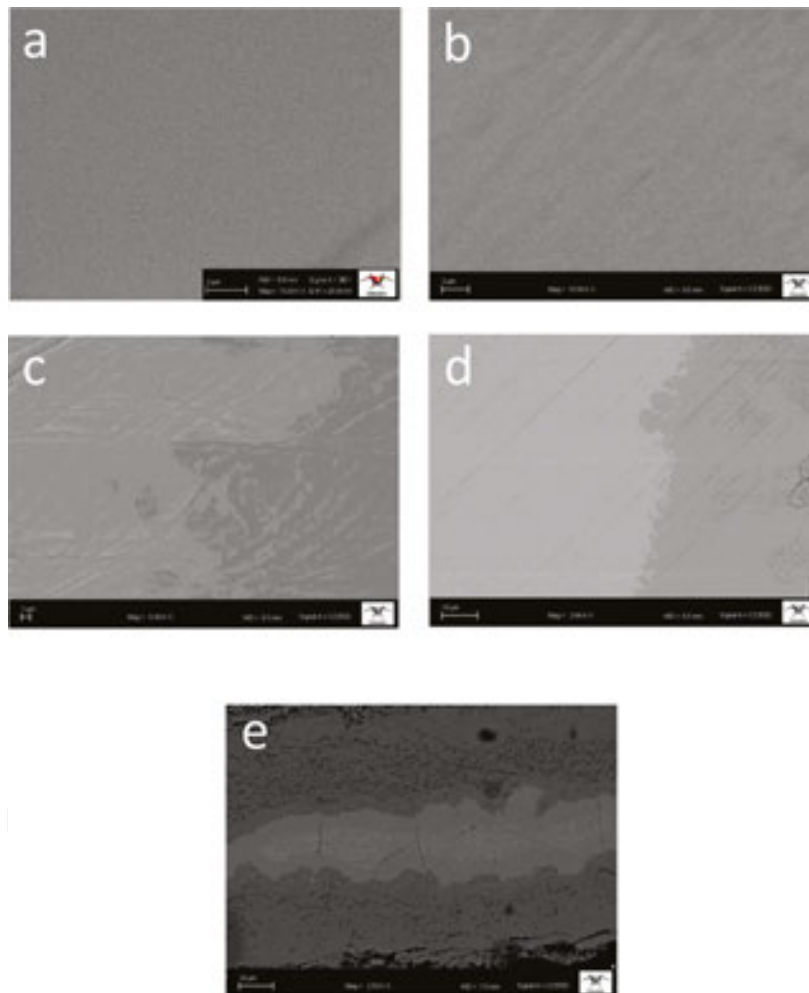


**Figure 6.** Typical SEM images from the cross section of the melt-spun ribbon of  $\text{Cu}_{50}\text{Zr}_{40}\text{Ni}_5\text{Al}_5$  alloy prepared at a wheel speed of  $35 \text{ ms}^{-1}$ . (a) As-quenched and annealed at the temperatures, (b) 300°C, (c) 580°C, (d) 680°C, and (e) 800°C.

The compositional homogeneity of the amorphous  $\text{Cu}_{50}\text{Zr}_{40}\text{Ni}_5\text{Al}_5$  ribbons was by measured EDX in order to confirm initially intended composition values. The EDX analysis illustrates mean values of element concentrations of  $\text{Cu}_{50}\text{Zr}_{40}\text{Ni}_5\text{Al}_5$  alloy produced at a wheel speed of

35 ms<sup>-1</sup> in **Figure 7**. As can be seen obviously from the EDX results, the peaks in the spectrum belong to Cu, Zr, Ni and Al elements. As shown in **Figure 7**, the average chemical composition of the ribbon alloy is in good agreement with the chemical composition values of Cu<sub>50</sub>Zr<sub>40</sub>Ni<sub>5</sub>Al<sub>5</sub> alloy.

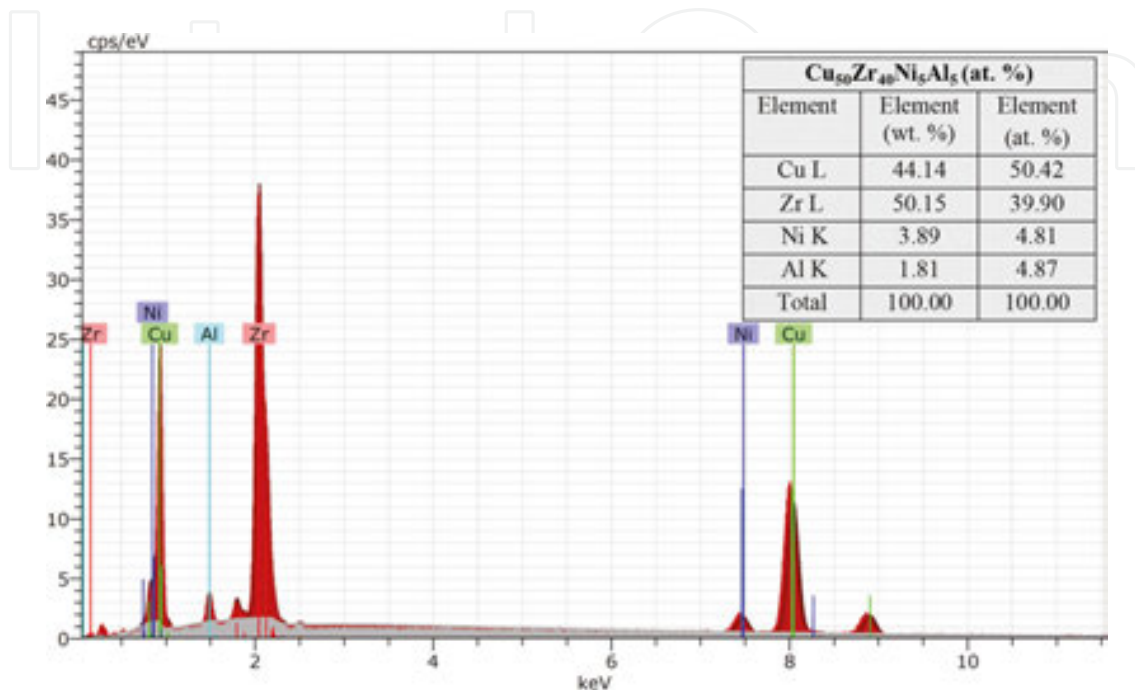


**Figure 7.** EDX analysis result of the melt-spun ribbon of Cu<sub>50</sub>Zr<sub>40</sub>Ni<sub>5</sub>Al<sub>5</sub> alloy produced at a wheel speed of 35 ms<sup>-1</sup> as-quenched.

In order to determine the influence of annealing on the microhardness of the Cu<sub>50</sub>Zr<sub>40</sub>Ni<sub>5</sub>Al<sub>5</sub> ribbon alloys which are as-quenched and annealed at different temperatures such as 200, 275, 400, 500, 600 and 800°C, Vickers HV measurements were analysed. The following Eq. (2) was used for these measurements [25]

$$HV = \frac{2P \sin(\theta/2)}{d^2} = \frac{1.8544(P)}{d^2} \quad (2)$$

where  $P$  is the indentation force,  $d$  is the mean diagonal length, and 1.854 is the geometrical factor for the diamond pyramid. **Figure 8** shows the variation of microhardness values with increasing annealing temperature for Cu<sub>50</sub>Zr<sub>40</sub>Ni<sub>5</sub>Al<sub>5</sub> alloy prepared at wheel speed of 35 ms<sup>-1</sup>. As shown in **Figure 8**, the hardness values decrease with increasing annealing temperature. In previous works, this decline of the hardness values with the annealing temperature is generally reported for Cu-based amorphous alloys [7, 26–31]. The microhardness of as-quenched ribbon was calculated 550 HV, while it was determined 532–470 HV for annealed ribbons in the range of 200–500°C (**Figure 8**). At the temperature range of 500–800°C, the

microhardness values of the  $\text{Cu}_{50}\text{Zr}_{40}\text{Ni}_5\text{Al}_5$  alloy were not changed distinctly and it was determined as approximately 465 HV. Thus, it can easily be concluded that the highest microhardness value (550 HV) of the  $\text{Cu}_{50}\text{Zr}_{40}\text{Ni}_5\text{Al}_5$  alloy was measured for as-quenched ribbon alloy.

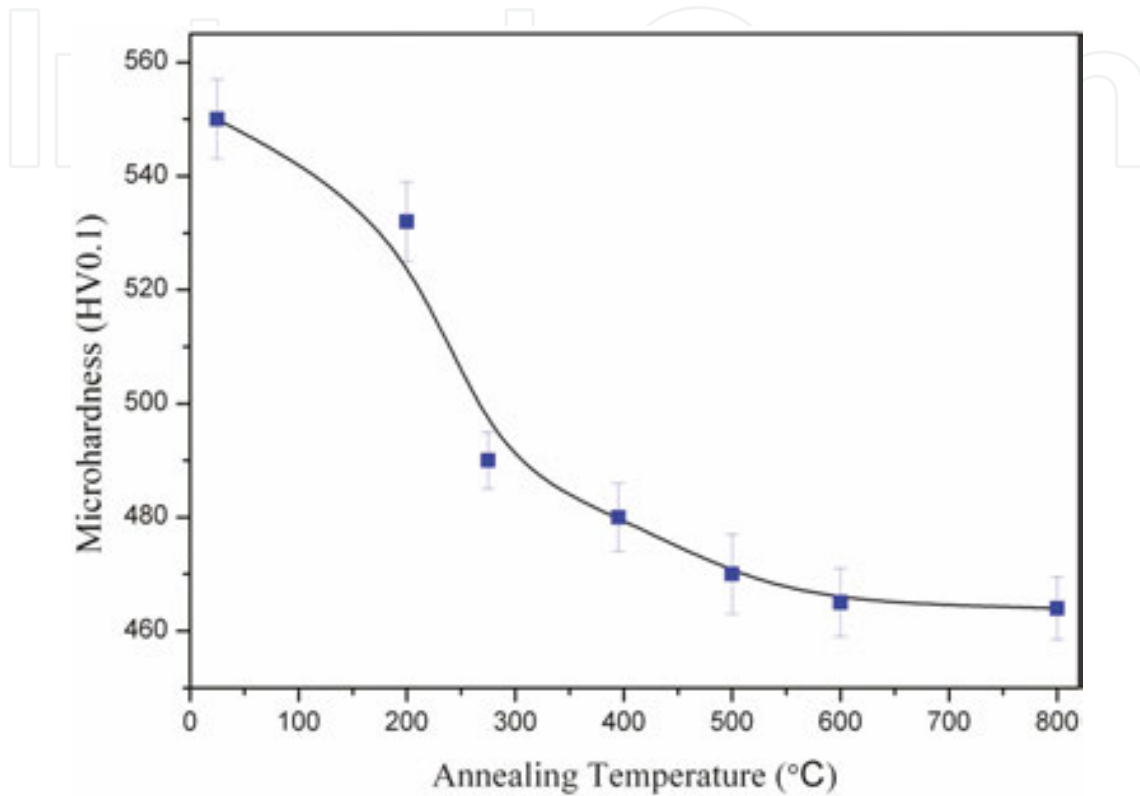


**Figure 8.** The change in Vickers microhardness values for  $\text{Cu}_{50}\text{Zr}_{40}\text{Ni}_5\text{Al}_5$  alloy prepared by the wheel speed of  $35 \text{ ms}^{-1}$  with annealing temperatures.

#### 4. Conclusions

1. The metallic glass  $\text{Cu}_{50}\text{Zr}_{40}\text{Ni}_5\text{Al}_5$  alloys were successfully produced by rapid solidification technique at wheel speeds of  $35$  and  $41 \text{ ms}^{-1}$ .
2. DSC traces of the  $\text{Cu}_{50}\text{Zr}_{40}\text{Ni}_5\text{Al}_5$  alloys showed similar distinct glass transition,  $T_g$  which are around  $440$ – $442^\circ\text{C}$ . The ribbon alloys exhibited also wide super-cooled liquid regions,  $\Delta T_x$  which are  $61$ – $64^\circ\text{C}$ .
3. The activation energies of  $E_g$ ,  $E_x$  and  $E_p$  for  $\text{Cu}_{50}\text{Zr}_{40}\text{Ni}_5\text{Al}_5$  alloy prepared at wheel speed of  $35 \text{ ms}^{-1}$  were determined  $421.35 (\pm 12)$ ,  $432.26 (\pm 9)$  and  $403.05 (\pm 6) \text{ kJ/mol}$ , respectively.
4. The intermetallic  $\text{AlCu}_2\text{Zr}$ ,  $\text{Cu}_{10}\text{Zr}_7$ ,  $\text{Zr}_2\text{Cu}$  and  $\text{Cu}$  phases in the microstructure of  $\text{Cu}_{50}\text{Zr}_{40}\text{Ni}_5\text{Al}_5$  alloy were observed after annealing temperature of  $800^\circ\text{C}$ .

5. The compositional homogeneity of  $\text{Cu}_{50}\text{Zr}_{40}\text{Ni}_5\text{Al}_5$  as-quenched ribbons was most correctly confirmed by EDX.
6. The microhardness value of  $\text{Cu}_{50}\text{Zr}_{40}\text{Ni}_5\text{Al}_5$  alloy was calculated approximately 550 HV for unannealed ribbons. However, it decreased with increasing annealing temperatures and was measured about 465 HV after annealing temperature of 800°C.

## Acknowledgements

We would like to thank Kahramanmaraş Sutcu Imam University for financial support of the research programme (Project No: 2014/3-34D). One of the authors (C. Kursun) would like to thank Council of Higher Education (YÖK) for graduate research support.

## Author details

Celal Kursun\* and Musa Gogebakan

\*Address all correspondence to: celalkursun@ksu.edu.tr

Department of Physics, Faculty of Art and Sciences, Kahramanmaraş Sutcu Imam University, Kahramanmaraş, Turkey

## References

- [1] A. Boutahara, H. Lassria, E.K. Hlib, D. Fruchart, Critical behavior and its correlation with magnetocaloric effect in amorphous  $\text{Fe}_{80-x}\text{V}_x\text{B}_{12}\text{Si}_8$  ( $x = 8, 10$  and  $13.7$ ) alloys. *Journal of Magnetism and Magnetic Materials*. 2016;398:26–31.
- [2] K. Tomolya, D. Janovszky, A. Sycheva, M. Sveda, T. Ferenczi, A. Roósz, Peculiarities of ball-milling induced crystalline–amorphous transformation in Cu–Zr–Al–Ni–Ti alloys. *Intermetallics*. 2015; 65:117–121.
- [3] Y. Ying-Jun, K. Fu-Wei, X. Da-Wei, S. Jian-Fei, S. Qing-Ke, S. Jun, Formation and mechanical properties of bulk Cu–Ti–Zr–Ni metallic glasses with high glass forming ability. *Transactions of Nonferrous Metals Society of China*. 2007;17:16–20.
- [4] C.K. Kim, H.S. Lee, S.Y. Shin, J.C. Lee, D.H. Kim, S. Lee, Microstructure and mechanical properties of Cu-based bulk amorphous alloy billets fabricated by spark plasma sintering. *Materials Science and Engineering: A*. 2005;406:293–299.
- [5] A. Inoue, K. Hashimoto, *Amorphous and nano-crystalline materials, preparation, properties and application*. Berlin: Springer, 2001.

- [6] M. Gogebakan, C. Kursun, J. Eckert, Formation of new Cu-based nanocrystalline powders by mechanical alloying technique. *Powder Technology*. 2013;247:172–177.
- [7] C. Kursun, M. Gogebakan, Y. Gencer, Microstructural characterization of rapidly solidified  $\text{Cu}_{50}\text{Zr}_{40}\text{Ni}_5\text{Ti}_5$  amorphous alloy. *Journal of Alloys and Compounds*. 2015;643:S33–S38.
- [8] A.M. Shams El Din, R.A. Mohammed, Contribution to the problem of vapour-side corrosion of copper–nickel tubes in MSF distillers. *Desalination*. 1998;115:135–144.
- [9] M. Weifang, L. Shuling, W. Jingtang, Isothermal crystallization kinetics of an amorphous CuTi alloy. *Chinese Journal of Metal Science and Technology*. 1992;8:197–203.
- [10] M. Gogebakan, C. Kursun, J. Eckert, Formation of new Cu-based nanocrystalline powders by mechanical alloying technique. *Powder Technology*. 2013;247:172–177.
- [11] J. Eckert, J. Das, K.B. Kim, F. Baier, M.B. Tang, W.T. Wang, Z.F. Zhang, High strength ductile Cu-based metallic glass. *Intermetallics*. 2006;14:876–881.
- [12] Y.J. Yang, R. Zhou, S.D. Wei, D.Y. Liu, H.L. Xu, S.L. Li, Microstructural evolution of slowly solidified Cu–Ti–Zr–Ni amorphous alloy. *Journal of Non-Crystalline Solids*. 2011;357:1516–1521.
- [13] S. Venkataraman, W. Loser, J. Eckert, T. Gemming, C. Mickel, P. Schulbert-Bischoff, N. Wanderka, L. Schultz, D.J. Sordelet, Nanocrystal development in  $\text{Cu}_{47}\text{Ti}_{33}\text{Zr}_{11}\text{Ni}_8\text{Si}_1$  metallic glass powders. *Journal of Alloys and Compounds*. 2006;415:162–169.
- [14] C.J. Hu, P.Y. Lee, Formation of Cu–Zr–Ni amorphous powders with significant supercooled liquid region by mechanical alloying technique. *Materials Chemistry and Physics*. 2002;74:13–18.
- [15] E.S. Park, H.K. Lim, W.T. Kim, et al. The effect of Sn on the glass-forming ability of Cu–Ti–Zr–Ni–Si metallic glass alloys. *Journal of Non-Crystalline Solids*. 2002;298:15–22.
- [16] J. Wu, Y. Pan, J. Huang, J. Pia, Non-isothermal crystallization kinetics and glass-forming ability of Cu–Zr–Ti–In bulk metallic glasses. *Thermochimica Acta*. 2013;552:15–22.
- [17] L. Liu, Z.F. Wu, J. Zhang, Crystallization kinetics of  $\text{Zr}_{55}\text{Cu}_{30}\text{Al}_{10}\text{Ni}_5$  bulk amorphous alloy. *Journal of Alloys and Compounds*. 2002;339:90–95.
- [18] H.E. Kissinger, Reaction kinetics in differential thermal analysis. *Analytical Chemistry*. 1957;29:1702.
- [19] Y.J. Yang, D.W. Xing, J. Shen, J.F. Sun, S.D. Wei, H.J. He, D.G. McCartney, Crystallization kinetics of a bulk amorphous Cu–Ti–Zr–Ni alloy investigated by differential scanning calorimetry. *Journal of Alloys and Compounds*. 2006;415:106–110.
- [20] L. Zhang, Z. HuaChen, Q. Zheng, D. Chen, Isochronal and isothermal phase transformation of  $\text{Cu}_{45}\text{Zr}_{45}\text{Ag}_7\text{Al}_3$  bulk metallic glass. *Physica B*. 2013;411:149–153.

- [21] D. Janovszky, A. Sycheva, K. Tomolya, J. Geiger, J. Solyom, A. Roos, Solidification processes in Cu–Zr–Ag amorphisable alloy system. *Journal of Alloys and Compounds*. 2014;584:600–606.
- [22] F.A. Javid, N. Mattern, S. Pauly, J. Eckert, Effect of cobalt on phase formation, microstructure, and mechanical properties of  $\text{Cu}_{50-x}\text{Co}_x\text{Zr}_{50}$  ( $x=2, 5, 10, 20$  at. pct) alloys. *Metallurgical and Materials Transactions A: Physical Metallurgy and Materials Science*. 2012;43:2631–2636.
- [23] C. Hu, P. Lee, Formation of Cu–Zr–Ni amorphous powders with significant supercooled liquid region by mechanical alloying technique. *Materials Chemistry and Physics*. 2002;74:13–18.
- [24] H. Yang, J.Q. Wang, Y. Li, Glass formation and microstructure evolution in Al–Ni–RE (RE=La, Ce, Pr, Nd and misch metal) ternary systems. *Philosophical Magazine*. 2007;87:4211–4228.
- [25] M. Gogebakan, O. Uzun, T. Karaaslan, M. Keskin, Rapidly solidified Al–6.5 wt% Ni alloy. *Journal of Materials Processing Technology*. 2003;142:87–92.
- [26] X. Mao, F. Fang, F. Yang, J. Jiang, R. Tan, Effect of annealing on microstructure and properties of Cu–30Ni alloy tube. *Journal of Materials Processing Technology*. 2009;209:2145–2151.
- [27] M.O. Prado, A. Tolley, Hardness of Cu–Mn–Al alloys as a function of the annealing temperature in the  $\beta$  phase. *Materials Science and Engineering A*. 1999;273–275:590–594.
- [28] Z. Wang, Y. Zhong, G. Cao, C. Wang, J. Wang, W. Ren, Z. Lei, Z. Ren, Influence of dc electric current on the hardness of thermally aged Cu–Cr–Zr alloy. *Journal of Alloys and Compounds*. 2009;479:303–306.
- [29] L. Huaqing, X. Shuisheng, M. Xujun, L. Yong, C. Lei, Influence of cerium and yttrium on Cu–Cr–Zr alloys. *Journal of Rare Earths*. 2006;24:367.
- [30] S. Suzuki, N. Shibutani, K. Mimura, M. Isshiki, Y. Waseda, Improvement in strength and electrical conductivity of Cu–Ni–Si alloys by aging and cold rolling. *Journal of Alloys and Compounds*. 2006;417:116–120.
- [31] Q. Lei, Z. Li, T. Xiao, Y. Pang, Z.Q. Xiang, W.T. Qiu, Z. Xiao, A new ultrahigh strength Cu–Ni–Si alloy. *Intermetallics*. 2013;42:77–84.